

## Article

# Indium Recovery by Adsorption on $\text{MgFe}_2\text{O}_4$ Adsorbents

Loredana Ciocărlie <sup>1</sup>, Adina Negrea <sup>1,\*</sup> , Mihaela Ciopec <sup>1</sup>, Narcis Duteanu <sup>1,\*</sup> , Petru Negrea <sup>1</sup>, Paula Ianasi <sup>2</sup>, Catalin Ianasi <sup>3</sup>  and Nicoleta Sorina Nemes <sup>4,\*</sup> 

<sup>1</sup> Faculty of Industrial Chemistry and Environmental Engineering, Polytechnic University of Timișoara, Victoriei Square, No. 2, 300006 Timișoara, Romania

<sup>2</sup> National Institute for Research and Development in Electrochemistry and Condensed Matter, 144th Dr. A.P. Podeanu Street, 300569 Timisoara, Romania

<sup>3</sup> “Coriolan Drăgulescu” Institute of Chemistry, Bv. Mihai Viteazul, No. 24, 300223 Timisoara, Romania

<sup>4</sup> Renewable Energy Research Institute—ICER, University Politehnica of Timisoara, 300501 Timisoara, Romania

\* Correspondence: adina.negrea@upt.ro (A.N.); narcis.duteanu@upt.ro (N.D.); nicoleta.nemes@upt.ro (N.S.N.)

**Abstract:** Indium and its compounds have many industrial applications and are widely used in the manufacture of liquid crystal displays, semiconductors, low temperature soldering, and infrared photodetectors. Indium does not have its own minerals in the Earth’s crust, and most commonly, indium is associated with the ores of zinc, lead, copper and tin. Therefore, it must be recovered as a by-product from other metallurgical processes or from secondary raw materials. The aim of this study is to investigate the adsorption properties for recovering indium from aqueous solutions using iron–magnesium composite ( $\text{MgFe}_2\text{O}_4$ ). In addition, the results show that the material offers very efficient desorption in 15% HCl solution, being used for 10 adsorption–desorption cycle test. These results provide a simple and effective process for recovering indium. Present study was focuses on the synthesis and characterization of the material by physico-chemical methods such as: X-ray diffraction, FT-IR spectroscopy, followed by the adsorption tests. The XRD indicates that the  $\text{MgFe}_2\text{O}_4$  phase was obtained, and the crystallite size was about 8 nm. New prepared adsorbent materials have a point of zero charge of 9.2. Studies have been performed to determine the influence of pH, initial indium solution concentration, material/solution contact time and temperature on the adsorption capacity of the material. Adsorption mechanism was established by kinetic, thermodynamic and equilibrium studies. At equilibrium a maximum adsorption capacity of 46.4 mg/g has been obtained. From kinetic and thermodynamic studies was proved that the studied adsorption process is homogeneous, spontaneous, endothermic and temperature dependent. Based on Weber and Morris model, we can conclude that the In (III) ions takes place at the  $\text{MgFe}_2\text{O}_4$ /In (III) solution–material interface.

**Keywords:** indium recovery; adsorption; iron oxide; magnesium oxide; composite



**Citation:** Ciocărlie, L.; Negrea, A.; Ciopec, M.; Duteanu, N.; Negrea, P.; Ianasi, P.; Ianasi, C.; Nemes, N.S. Indium Recovery by Adsorption on  $\text{MgFe}_2\text{O}_4$  Adsorbents. *Materials* **2022**, *15*, 7054. <https://doi.org/10.3390/ma15207054>

Academic Editor: Gianfranco Dell’Agli

Received: 17 August 2022

Accepted: 6 October 2022

Published: 11 October 2022

**Publisher’s Note:** MDPI stays neutral with regard to jurisdictional claims in published maps and institutional affiliations.



**Copyright:** © 2022 by the authors. Licensee MDPI, Basel, Switzerland. This article is an open access article distributed under the terms and conditions of the Creative Commons Attribution (CC BY) license (<https://creativecommons.org/licenses/by/4.0/>).

## 1. Introduction

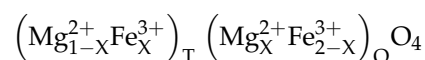
Indium and its compounds have widespread industrial applications in several fields [1,2]. The European Union included indium into the list of critical materials. China was reported as one the largest producers of indium in the world, reaching a total of 290 tons in 2016. For example, in 2009 about 110 tons of indium were consumed in the US, and indium consumption increases annually [1–6]. Massive development of mobile electronic devices requires a large consumption of In, used in the form of indium–tin–oxide layers into LCD construction [7]. Different estimations indicate that into the Earth’s crust indium content ranges from 50 to 200 parts per billion [8]. However, at the present consumption rate indium reserves are expected to be depleted in 20 years, and the demand and consumption of indium increases every year [9,10]. Until now, different attempts were made for In recovery from different scraps [7]. Therefore, the development of an efficient recovery process is extremely important for the stable supply of indium, along with the issue of resource recycling and environmental sustainability [11–13].

Conventional methods for recovering indium from secondary resources (such as industrial wastewater), include precipitation [2,14,15], solvent extraction [16], ion exchange [2,10,17–21], nanofiltration membranes [2,22], chemical reduction [2,23], and electroanalytical techniques [2,24]. Solvent precipitation and solvent extraction are well-known recovery methods, but they generate potential environmental problems caused by the usage of large amounts of chemicals and organic solvents [17]. However, the principal disadvantage of the solvent extraction process is represented by extractant loss, which can cause environmental hazards concomitant with economic constraints. Compared to solvent extraction, ion exchange technique is much easier. However, its low selectivity for desired metallic ions represents the main problem of such a recovery technique. Recently, the usage of impregnated resins was developed as a technological alternative for indium ion extraction [10,25–28]. Other technologies used for indium recovery from aqueous solutions are solvent extraction and resin adsorption. In order to attain a higher separation efficiency of indium from aqueous solutions it is recommended to use multi-step extraction/adsorption and reverse extraction/desorption. In addition, an increase in secondary waste production was observed when of organic solvent and acidic solutions introduction.

The pyrometallurgical method can be used for recovery of indium species, but it needs a large amount of energy to operate at high temperatures, and its ability to separate metals is not ideal. Electroplating has a high operability due to the controllable potential of the electrode and the adjustable electroreduction property of the metal by the addition of ligand [29,30] and demonstrated superiority in the extraction of metal from multimetallic waste.

Adsorption is expected to be the most suitable method for recovering indium due to its simple concept, high safety and ecological process [14,31–35]. In particular, different research studies were carried out in order to find a proper adsorbent material, with higher selectivity for indium ions. Such materials are represented by different polymeric resins, having grafted different functional groups [9,36]. Fortes et al. reported adsorption of indium in aqueous solution by means of chelating resin of iminodiacetic acid as a sorbent [2,37], and Tokuyama and Iwama studied solid phase extraction of indium using poly (N-isopropylacrylamide) as the sorbent [38]. The hydrogen ion of the iminodiacetic acid group on the polymeric resin could be replaced with the indium ions. In this way, indium ions are displaced and chelated inside the polymeric resin by the functional group [37]. Moreover, Calagui et al. [14], reported the adsorption of indium from aqueous solution on chitosan-coated bentonite balls. Therefore, numerous adsorptive processes have been developed for indium separation and recovery from different residual solutions. In such processes, various absorbents were used such as: starch, activated carbon, activated carbon clothing, fly ash, chitin, shrimp shell, peanut shell pellets, clay minerals, zeolites and resins [2,14,39–46].

In the present paper we describe the attempt of usage of magnesium ferrites spinel type structure as an adsorbent material for indium recovery. Until now, usage of  $\text{MgFe}_2\text{O}_4$  spinel as adsorbent material has been very limited. The spinel-type structures of magnesium ferrites are of increasing interest due to their chemical and physical properties. The molecular structure of magnesium ferrites is found in the form of:



$\text{Mg}^{2+}$ ,  $\text{Fe}^{3+}$ —divalent and trivalent cations  
X—degree of inversion

In a spinel structure, cations  $\text{Mg}^{2+}$  and  $\text{Fe}^{3+}$  can occupy tetrahedral interstitial positions (T) as well as octahedron (O) of the cubic lattice formed by ions of  $\text{O}^{2-}$  [47]. Bloesser et al. shows that in order to obtain materials with the desired properties we have to change the degree of inversion by modifying the synthesis parameters [48]. If we change parameters such as temperature, the interstitial positions of magnesium ions can also change.

Hammache et al. indicate that the spinel  $\text{MgFe}_2\text{O}_4$  is non-toxic to the environment [49]. From the data of the literature it was observed that the spinel  $\text{MgFe}_2\text{O}_4$  presents a wide range of applications such as: photocatalysis [50], catalytic activity, gas sensor, electronics, battery anode, pigments, magnetic resonance imaging, hyperthermia therapy and targeted drug delivery.

Various methods can be used to obtain ferrite spinel such as sol-gel, pulse laser deposition, hydrothermal [49], coprecipitation [47], microemulsions, combustion method and solid-state reaction [51]. The aim of this study is to investigate the adsorptive properties of spinel type magnesium ferrites for indium recovery from aqueous solutions.

## 2. Materials and Methods

### 2.1. Material Synthesis and Characterization

#### 2.1.1. $\text{MgFe}_2\text{O}_4$ Composite Synthesis

$\text{MgFe}_2\text{O}_4$  composite was prepared by coprecipitation method [52]. Thus, to obtain the composite adsorbent 1 g of magnesium carbonate,  $\text{MgCO}_3$  (SC CHIMOPAR TRADING SRL, Bucharest, Romania), 30 mL of distilled water together with 30 mL of methanol (SC CHIMOPAR TRADING SRL, Bucharest, Romania) were contacted, mixed for 1 h and then 5 mL of  $\text{HNO}_3$  solution (SC CHIMOPAR TRADING SRL, Bucharest, Romania) was added to reach a pH between 1.5 and 2. The  $\text{HNO}_3$  solution is made by adding 5 mL of concentrated  $\text{HNO}_3$  and 245 mL of distilled water. After another half hour, the iron (III) nitrate,  $\text{Fe}(\text{NO}_3)_3$  (SC CHIMOPAR TRADING SRL, Bucharest, Romania) was added, the temperature raised to 50 °C and the solution was stirred until it was homogenous, after about 3 h. To precipitate the material at the end, ~10 mL of NaOH solution (Merck, Sigma Aldrich, Munchen, Germany) was added to increase the pH to 5. The NaOH solution was made by adding 7.5 g of NaOH beads in 100 mL of distilled water. After obtaining the precipitate, the supernatant was removed. To remove Na from the compound it was washed with excess water. The material was dried for 24 °C to 100 °C in an oven (Pol-eko model SLW 53, SDT, Rybnik, Poland), then calcined at 260 °C in an oven at a speed of 5° /min, using an oven with controlled air atmosphere (Nabertherm LHT407GN Furnaces, Lilienthal, Germany).

#### 2.1.2. $\text{MgFe}_2\text{O}_4$ Composite Physico-Chemical Characterization

##### Thermogravimetric Analysis, DTG

The differential thermal analysis, DTG, was performed to highlight the temperature dependence of the physical properties, using a TGA/SDTA 851-LF Mettler-Toledo. The decomposition was performed in the presence of air and the sample was heat treated in the range of 25–900 °C.

##### Fourier Transform Infra-Red Spectroscopy, FT-IR

The material was characterized by Fourier transform infrared spectroscopy (FT-IR) by using a JASCO FT/IR-4200 apparatus (SpectraLab, Shimadzu, Japan).

##### X-ray Diffraction Analysis, XRD

In order to obtain information about the degree of crystallinity of the material and the presence of several phases in the material, X-ray diffraction analysis was performed, XRD (D8 Advance-Bruker AXS), using Mo-K $\alpha$  radiation ( $\lambda_{\text{Mo}} = 0.7093 \text{ \AA}$ ).

##### $\text{pH}_{\text{pZc}}$

Point of zero charge,  $\text{pH}_{\text{pZc}}$ , was determined by bringing the studied system to equilibrium. In this case, 0.1 g of adsorbent material ( $\text{MgFe}_2\text{O}_4$ ) wZ mixed with 25 mL of 0.1 N KCl solution at 200 rpm and a temperature of 298 K, using a water bath with thermostating and stirring, Julabo SW23 type. KCl solutions pH was modified in range 2–12, by adding NaOH solutions with a concentration between 0.05 N and 2 N or  $\text{HNO}_3$  solutions with a concentration between 0.05 N and 2 N. Further, all the samples were

filtered and subsequently was determined the pH of the resulting solution by using a pH meter (METTLER TOLEDO, SevenCompact, S 210 type).

### 2.1.3. Adsorption Studies pH Effect

In the present paper we studied the influence of pH on the adsorption process of In (III) on the synthesized material, varying the pH, in the range 1–14. Thus, 0.1 g of material was kept in contact with 25 mL of In (III) solution (InCl<sub>3</sub>, 99.995% purity, ACROS organics, India) of initial concentration,  $C_0 = 100 \mu\text{g L}^{-1}$ , for 60 min in a JUABO type thermostatic bath (SW 23), at a temperature of 298 K. The pH of the solutions was adjusted using HNO<sub>3</sub> and NaOH solutions having concentrations in the range of 0.1–1 N, obtained by diluting 63% HNO<sub>3</sub> (Carl Roth) and NaOH, pellets (Merck Sigma Aldrich).

### Contact Time and Temperature Effect

In order to establish the influence of contact time and temperature on material adsorption capacity, 0.1 g of adsorbent material were weighed and mixed with a 25 mL solution containing  $100 \mu\text{g L}^{-1}$  In (III). Different samples were prepared, which were mixed for different times (15, 30, 60 and 120 min), at different temperatures (298, 308, 318 and 328 K) and 200 rpm using a thermostatic bath.

### Initial Concentration Effect

In order to establish the effect of the initial concentration of In (III) ions on the adsorption capacity of the MgFe<sub>2</sub>O<sub>4</sub> adsorbent material, solutions with concentrations of  $5 \times 10^2$ ,  $1 \times 10^3$ ,  $1.5 \times 10^3$ ,  $2 \times 10^3$ ,  $3 \times 10^3$ ,  $5 \times 10^3$ ,  $7 \times 10^3$ ,  $8 \times 10^3$ ,  $1 \times 10^4$ ,  $5 \times 10^4$ ,  $1 \times 10^5$ ,  $2 \times 10^5$  and  $3 \times 10^5 \mu\text{g L}^{-1}$  were prepared. These solutions were prepared by appropriate dilution from a stock solution of InCl<sub>3</sub>,  $1000 \text{ mg L}^{-1}$ . All adsorption tests were conducted at pH > 2 for 90 min and at 298 K. In order to evaluate the adsorption capacity was measured the residual concentration of In (III), by using the graphite furnace atomic absorption spectrophotometer (AA 6800, Shimadzu).

### Kinetics Adsorption

In order to study the adsorption kinetic for studied adsorption process obtained experimental data were modelled with three different kinetic models: Lagergren, Ho and McKay, and Weber and Morris one. Equations used to describe adsorption kinetic are presented in Table 1.

**Table 1.** Equations used to describe adsorption kinetics.

Parameters	Equation	References
Pseudo-first order kinetic model (Lagergren)	$\ln(q_e - q_t) = \ln q_e - k_1 t \quad (1)$ where: $q_e$ —equilibrium adsorption capacity ( $\text{mg g}^{-1}$ ) $q_t$ —adsorption capacity at a specific time— $t$ ( $\text{mg g}^{-1}$ ) $k_1$ —pseudo-first order speed constant ( $\text{min}^{-1}$ ) $t$ —contact time (min)	[53]
Pseudo-second order kinetic model (Ho and McKay)	$\frac{t}{q_t} = \frac{1}{k_2 q_e^2} + \frac{t}{q_e} \quad (2)$ $q_e$ —equilibrium adsorption capacity ( $\text{mg g}^{-1}$ ) $q_t$ —adsorption capacity at a specific time— $t$ ( $\text{mg g}^{-1}$ ) $k_2$ —pseudo-second order speed constant ( $\text{g mg}^{-1} \text{min}^{-1}$ ) $t$ —contact time (min)	[54,55]
Intraparticle diffusion (Weber and Morris model)	$Q_t = k_{diff} \cdot t^{1/2} + C \quad (3)$ where: $Q_t$ —adsorption capacity at $t$ time, $\mu\text{g/g}$ $k_{diff}$ —speed constant for intraparticle diffusion, $\mu\text{g/g} \cdot \text{min}^{1/2}$ $C$ —constant correlated with the thickness of the liquid film surrounding the adsorbent particles.	[56,57]

### Adsorption Isotherm Models

Similar, in order to better understand and describe the adsorption equilibrium, experimental data were modelled using Langmuir, Freundlich and Sips isotherms. Equations used to describe adsorption equilibrium are presented in Table 2.

**Table 2.** Equations used to describe adsorption equilibrium.

Parameters	Equation	References
The adsorption capacity of the material	$q_e = \frac{(C_0 - C_e) V}{m} \quad (4)$ where: $q_e$ —the maximum adsorption capacity ( $\mu\text{g g}^{-1}$ ) $C_0$ —initial concentration of metallic ion in solution ( $\mu\text{g L}^{-1}$ ) $C_e$ —the equilibrium concentration of metallic ion in solution ( $\mu\text{g L}^{-1}$ ) $V$ —volume of the aqueous solution with metallic ion content (L) $m$ —mass of the adsorbent (g)	
Langmuir isotherm nonlinear expression	$q_e = \frac{q_L K_L C_e}{1 + K_L C_e} \quad (5)$ where: $q_e$ —the maximum adsorption capacity ( $\mu\text{g g}^{-1}$ ) $C_e$ the equilibrium concentration of metallic ion in solution ( $\mu\text{g L}^{-1}$ ) $q_L$ —Langmuir maximum adsorption capacity ( $\mu\text{g g}^{-1}$ ) $K_L$ —Langmuir constant	[58]
Freundlich isotherm nonlinear expression	$q_e = K_F C_e^{1/n_F} \quad (6)$ where: $q_e$ —the maximum adsorption capacity ( $\mu\text{g g}^{-1}$ ) $C_e$ —the equilibrium concentration of metallic ion in solution ( $\mu\text{g g}^{-1}$ ) $K_F$ and $n_F$ —the characteristic constants that can be related to the relative adsorption capacity of the adsorbent and the intensity of adsorption	[35]
Sips isotherm nonlinear expression	$q_e = \frac{q_s K_S C_e^{1/n_S}}{1 + K_S C_e^{1/n_S}} \quad (7)$ where: $q_s$ —the maximum adsorption capacity ( $\mu\text{g g}^{-1}$ ) $K_S$ —constant related to the adsorption capacity of the adsorbent $n_S$ —the heterogeneity factor	[59]

### Thermodynamic Studies

The amount of activation energy,  $E_a$ , provides information about the nature of the adsorption process whether it is physical or chemical. Further, starting from the experimental data obtained for In (III) adsorption on the prepared adsorbent, we evaluated the activation energy based on the Arrhenius equation:

$$\ln k_2 = \ln A - \frac{E_a}{RT} \quad (8)$$

where:

$k_2$ —speed constant ( $\text{g min}^{-1} \text{mg}^{-1}$ )

$A$ —Arrhenius constant ( $\text{g min mg}^{-1}$ )

$E_a$ —activation energy ( $\text{kJ mol}^{-1}$ )

$T$ —absolute temperature (K)

$R$ —ideal gas constant ( $8.314 \text{ J mol}^{-1} \text{K}^{-1}$ ).

Taking in account that the pseudo-second-order model is better fitting obtained experimental data, the activation energy was calculated by using the speed constant obtained based on this model. Based on the slope of the linear dependence  $\ln k_2$  versus  $1/T$ , was determined the value of activation energy.

Further, based on Gibbs–Helmholtz equation was calculated the value of Gibbs energy, used to establish if the In (III) adsorption onto the prepared adsorbent material is a spontaneous process [33]:

$$\Delta G^\circ = \Delta H^\circ - T \cdot \Delta S^\circ \quad (9)$$

where:

$\Delta G^\circ$ —free Gibbs energy standard variation ( $\text{J mol}^{-1}$ )

$\Delta H^\circ$ —enthalpy standard variation ( $\text{J mol}^{-1}$ )

$\Delta S^\circ$ —entropy standard variation ( $\text{J mol}^{-1} \text{K}^{-1}$ )

T—absolute temperature (K)

Standard variations of enthalpy and entropy were evaluated from linear dependence of  $\ln K_d$  versus  $1/T$  (linear form of van't Hoff equation), where  $K_d$  is the equilibrium constant, which was calculated as ratio between equilibrium adsorption capacity ( $q_e$ ) and equilibrium concentration ( $C_e$ ).

### 3. Results and Discussion

#### 3.1. Material Synthesis and Characterization

##### 3.1.1. Thermogravimetric Analysis, DTG

Figure 1 shows that the material decomposes in three steps. In the first part of the process up to 200 °C there are two specific peaks associated with elimination of water and organic solvents with a mass loss of 16.35%. In the second part of the process an exothermic process takes place, attributed to iron nitrate III beginning to decompose, and  $\text{NO}_x$  is formed. At the same time, the decomposition of  $\text{MgCO}_3$  and  $\text{CO}_2$  takes place [60].

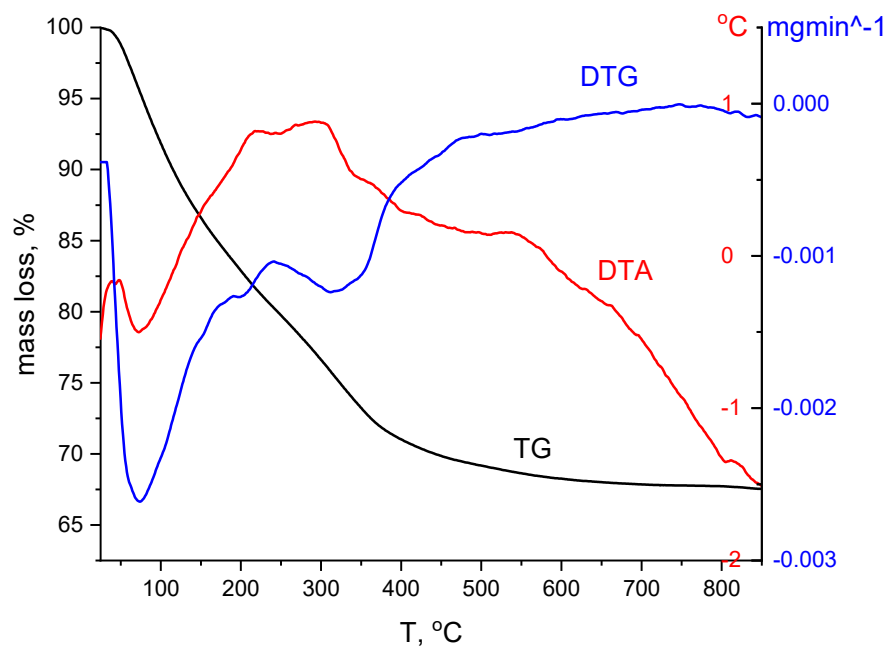


**Figure 1.** Thermogravimetric analysis for  $\text{MgFe}_2\text{O}_4$  material.

At this stage in the range of 200–500 °C there is a loss of 14.49% with the formation of the spinel  $\text{MgFe}_2\text{O}_4$  and partially a crystalline phase of  $\text{Fe}_3\text{O}_4$ . In the last stage, the material has a loss of about 1.78%. At a temperature of 875 °C, the material has a plateau meaning that most of the processes have taken place.

Chemical analysis was performed after calcination of the sample up to 900 °C indicating that Mg and Fe ions are in ideal proportions for the formation of  $\text{MgFe}_2\text{O}_4$ .

### 3.1.2. X-ray Diffraction Analysis, XRD

Figure 2 shows X-ray diffractograms for  $\text{MgFe}_2\text{O}_4$  powder calcined at  $260\text{ }^\circ\text{C}$ .

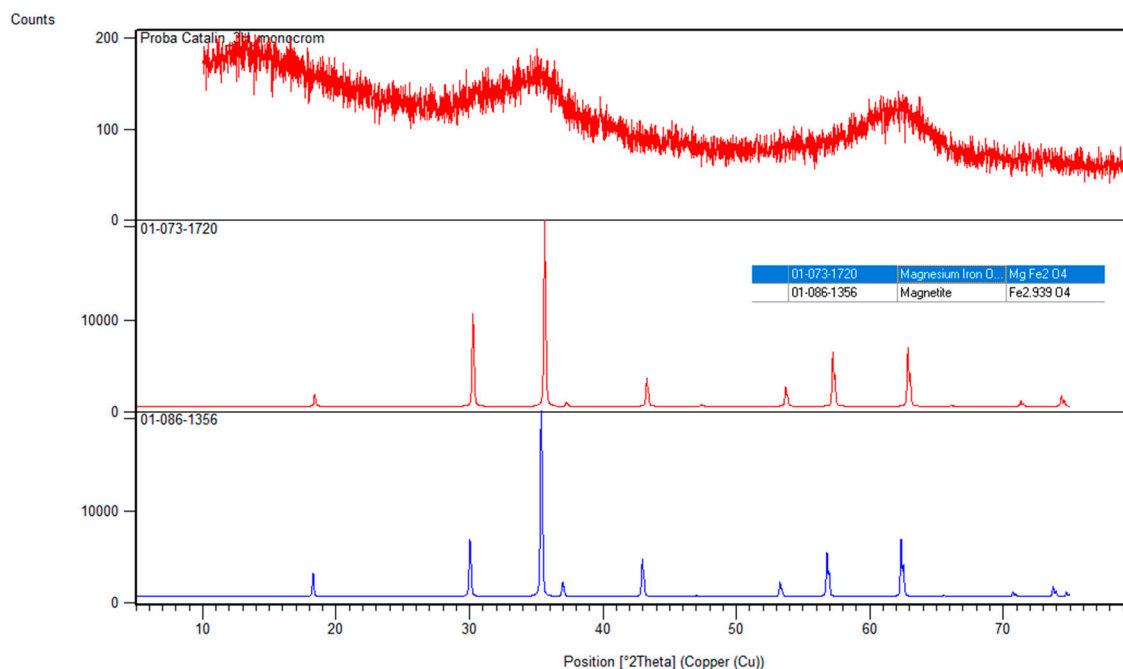


**Figure 2.** XRD  $\text{MgFe}_2\text{O}_4$  material treated at  $260\text{ }^\circ\text{C}$ .

The general appearance of the material is that it is amorphous, but following the peaks from  $30$ ,  $35$ ,  $57$  and  $63$ ,  $2\theta$ , which are associated with the presence of the crystalline phases  $220$ ,  $311$ ,  $333$  and  $440$ , can conclude that a  $\text{MgFe}_2\text{O}_4$  phase was obtained. The material corresponds to a cubic-type network,  $\text{Fd-}3\text{m}$ . The sampled data were evaluated using the reference sheet  $01-073-1720$  indicating that the major phase  $\text{MgFe}_2\text{O}_4$ . A secondary phase is formed to a small extent being specific to magnetite. Using Scherrer's equation, the crystallite size was determined using the peaks at  $311$  and  $440$  with an average value of about  $8\text{ nm}$ .

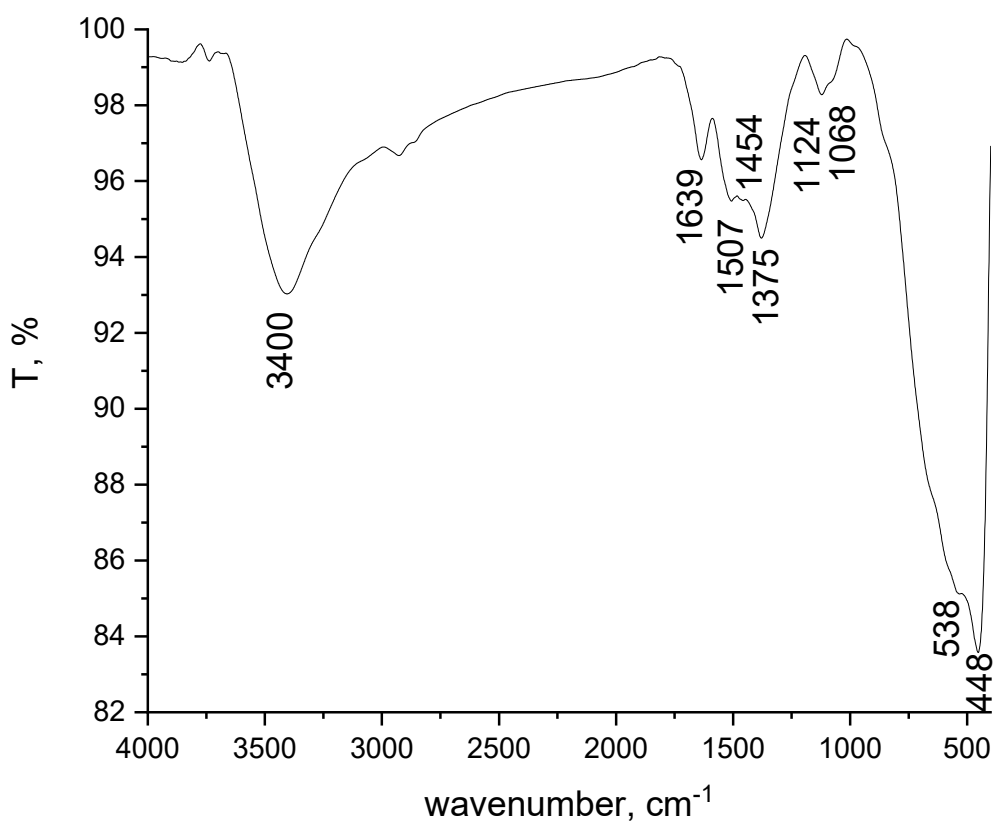
### 3.1.3. FT-IR Spectra

Figure 3 shows the FT-IR spectrum of the  $\text{MgFe}_2\text{O}_4$  material, recorded into the range  $4000$  and  $400\text{ cm}^{-1}$ .

By analysing the spectrum depicted in Figure 3 the presence of the specific bands for  $-\text{OH}$  stretching and bending vibrations are observed, located at  $3400$  and  $1639\text{ cm}^{-1}$ , respectively [47]. The  $1507$ ,  $1454$  and  $1375\text{ cm}^{-1}$  bands specific for stretching vibration of carbon groups are also present in the spectrum. The adsorption band at  $1124$  and  $1068\text{ cm}^{-1}$  could be attributed to the presence of nitrates ion [61].

The most important bands obtained at  $538$  and  $448\text{ cm}^{-1}$  are specific for the formation of the spinel ferrite structure. Referring to the literature, we note that in the peak located at  $448\text{ cm}^{-1}$ , it is specific for octahedral  $\text{Mg-O}$  and  $\text{Fe-O}$ . In our case, the peak at  $538\text{ cm}^{-1}$  shows the clear formation of spinel  $\text{MgFe}_2\text{O}_4$  or/and tetrahedral  $\text{Fe-O}$  [62,63].

These absorbance bands are attributed to vibration of tetrahedral (higher energy band of  $\text{M-O}$ ) and octahedral (lower frequency band of  $\text{M-O}$ ) complexes, respectively [64,65].



**Figure 3.** FT-IR spectra of the MgFe<sub>2</sub>O<sub>4</sub> composite.

#### 3.1.4. Point of Zero Charge (pH<sub>pZc</sub>) Determination

The value of point of zero charge (pH<sub>pZc</sub>) was determined using the so-called method “11 points” [66], which was also used by Freitas et al. in their studies [34]. pH<sub>pZc</sub> is defined as the value where the final pH remains constant [34,67]. The pZc is determined using the graphical representation of the initial pH vs. final pH (Figure 4).

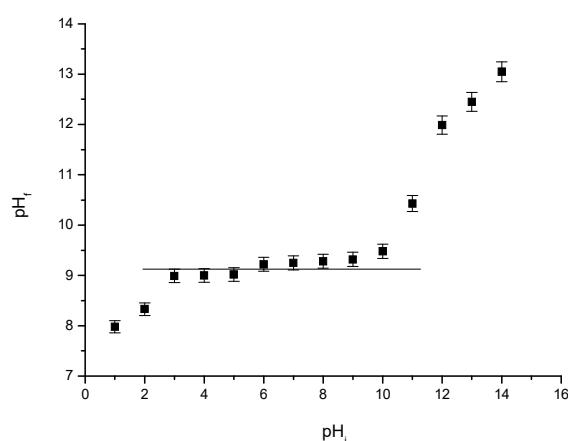


**Figure 4.** pH<sub>pZc</sub> for MgFe<sub>2</sub>O<sub>4</sub> material treated at 260 °C.

In our case the pH<sub>pZc</sub> is 9.2. This is considered to be the ideal working pH. pZc value represents a clear indication of whether the adsorbent material surface is positively or negatively charge, and depends on the pH value [67].

### 3.2. Adsorption Studies

#### 3.2.1. pH Effect

The pH effect of the In (III) adsorption is shown in Figure 5.

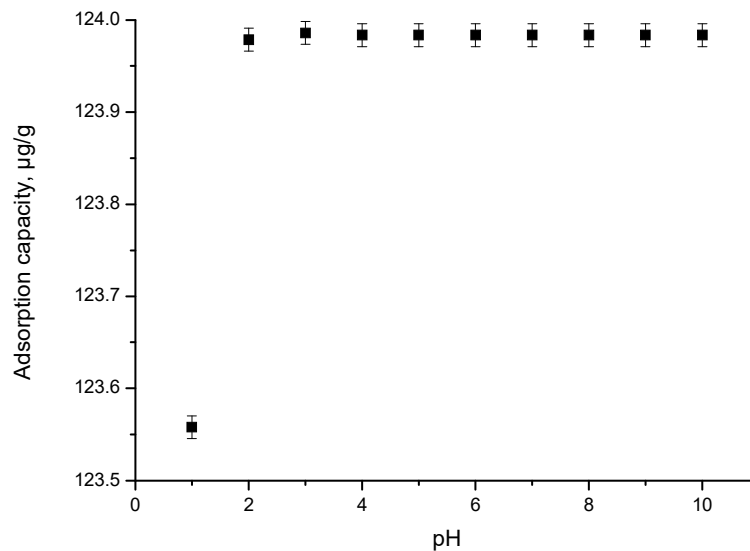


Figure 5. pH effect.

It is observed that at  $\text{pH} < 2$ , the adsorption capacity increases with the pH increase, reaching a maximum value of  $124 \mu\text{g In (III)}/\text{g MgFe}_2\text{O}_4$  at pH 2. By any further increase in the pH value, one can observe that the adsorption capacity remains constant. At a pH value lower than 2, according to the literature data, specific species of In (III) coexisting in solution can be:  $\text{In(OH)}_3^0$ ;  $\text{In(OH)}_2^+$  or  $\text{In(OH)}_4^-$  [68,69].

#### 3.2.2. Contact Time and Temperature Effect

The effect of contact time (between 15–120 min) at four different temperatures (298, 308, 318 and 328 K) was studied (obtained data are depicted in Figure 6).

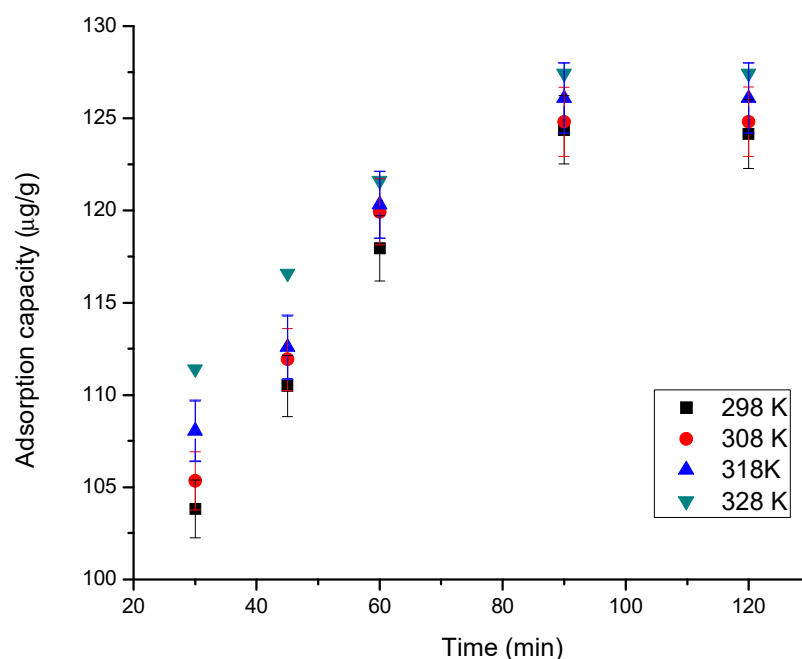


Figure 6. Contact time and temperature effect.

The results obtained indicate that by increasing the contact time,  $MgFe_2O_4$  adsorption capacity increases. Moreover, it can be observed that the constant adsorption capacity is reached ( $\sim 125 \mu g \text{ In (III)}/g$ ) after 90 min [70]. With increasing temperature, the adsorption capacity increases, but insignificantly, which is why subsequent studies are performed only at 298 K.

### 3.2.3. Kinetic Studies

Kinetics of In (III) adsorption on  $MgFe_2O_4$  material was also evaluated. For that, obtained experimental data were modelled using the equations of the pseudo-first-order and pseudo-second-order kinetic models (Figure 7a,b). To distinguish whether film diffusion or intraparticle diffusion it is the speed determinant step, obtained experimental data were modelled according to the Weber and Morris model, studying intraparticle diffusion (Figure 7c).

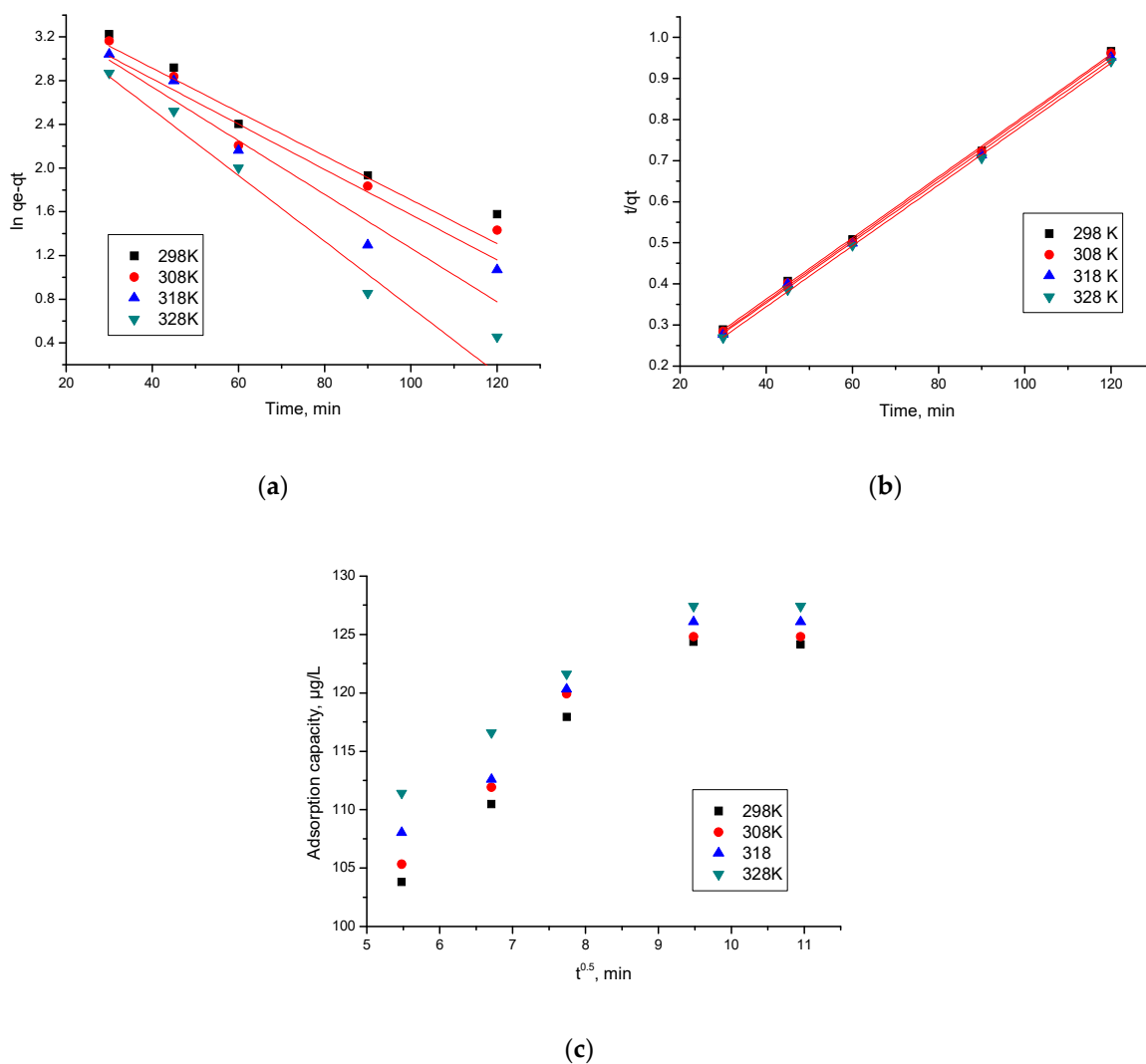


Figure 7. Kinetic studies. (a) Pseudo-first order; (b) pseudo-second order; (c) intraparticle diffusion.

Based on the results obtained from modelling, were evaluated the values of the speed constants, as well as the values obtained for the diffusion coefficient and C parameters, data presented in Table 3. Withal were calculated the values of the regression coefficient,  $R^2$  (depicted in same table).

**Table 3.** Kinetic parameters for the adsorption of In (III) onto MgFe<sub>2</sub>O<sub>4</sub>.

Pseudo-First-Order				
Temperature (K)	$q_{e,exp}$ ( $\mu\text{g g}^{-1}$ )	$k_1$ ( $\text{min}^{-1}$ )	$q_{e,calc}$ ( $\mu\text{g g}^{-1}$ )	$R^2$
298	124.3	0.020	39.61	0.8930
308	125.0	0.022	41.15	0.8883
318	126.0	0.023	41.63	0.9063
328	127.4	0.030	42.17	0.9114
Pseudo-second-order				
Temperature (K)	$q_{e,exp}$ ( $\mu\text{g g}^{-1}$ )	$k_2$ ( $\text{g } \mu\text{g}^{-1} \cdot \text{min}^{-1}$ )	$q_{e,calc}$ ( $\mu\text{g g}^{-1}$ )	$R^2$
298	124.3	197.7	113.6	0.9991
308	125.0	234.2	119.0	0.9992
318	126.0	276.2	126.5	0.9992
328	127.4	342.4	128.2	0.9996
Intraparticle diffusion model (IPD)				
Temperature (K)	$K_{diff}$ ( $\mu\text{g} \cdot \text{g}^{-1} \text{ min}^{-1/2}$ )	C	$R^2$	
298	3.06	84.7	0.8646	
308	3.54	87.7	0.8370	
318	3.67	90.0	0.8721	
328	3.88	96.1	0.8646	

From the data depicted in Table 3, it can be seen that obtained experimental data are modelled well by the pseudo-second-order kinetic model, proved by the regression coefficient value closer to one,  $R^2 \sim 1$  (0.9991–0.9996). When obtained experimental data were modelled according to the pseudo-first-order kinetic model one,  $R^2$  is between 0.8930 and 0.9114. Moreover, the value of  $q_{e,calc}$  calculated based on the pseudo-second-order isotherm it is close to the experimental one ( $q_{e,exp}$ ). Values of the calculated parameters ( $k_2$ ,  $q_{e,calc}$ ) are influenced by the temperature value, but not significantly, so it is not necessary to work at temperatures higher than 298 K.

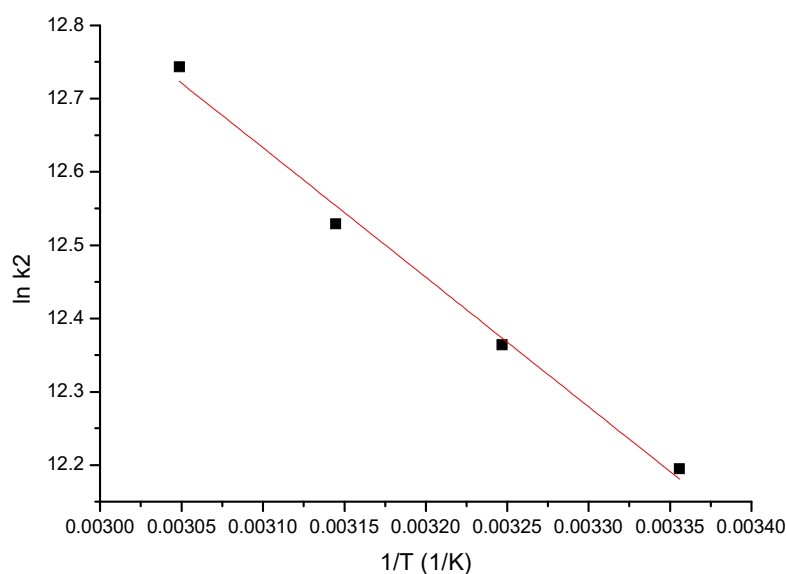
At the same time, it is observed that the adsorption mechanism of In (III) is taking place in several stages, because the line obtained by the graphical representation of the dependence of  $q_t = f(t^{1/2})$  at different temperatures, are not passing through the origin ( $C = 0$ ). Thus, we can say that both intraparticle diffusion and film diffusion influence the kinetics of adsorption. From the data presented in Table 4 it is observed that with increasing temperature the  $K_{diff}$  value also increases. It is also observed that, specific to stage 1, the diffusion constants are higher than the diffusion constants specific to stage 2, which allows us to state that the determinant of velocity is stage 1 and that in stage 2 the process is slower [71].

### 3.2.4. Activation Energy

The value of the activation energy,  $E_a$ , offers information about the nature of the adsorption process, whether it is a physical or chemical one. This is calculated based on graphical representation of  $\ln K_2$  vs.  $1/T$ , based on Arrhenius' equation (Figure 8). In the case of the studied process (In (III) adsorption on the MgFe<sub>2</sub>O<sub>4</sub> material), the activation energy  $E_a$  was calculated, using the rate constant from the pseudo-second-order kinetic model  $k_2$ .

**Table 4.** Parameters of isotherm model for adsorption In (III) onto MgFe<sub>2</sub>O<sub>4</sub>.

Langmuir Isotherm			
$q_{m,exp} (\mu\text{g g}^{-1})$	$K_L (\text{L } \mu\text{g}^{-1})$	$q_L (\mu\text{g g}^{-1})$	$R^2$
46,396	$3.84 \times 10^{-4}$	51,616	0.9717
Freundlich isotherm			
$K_F (\mu\text{g g}^{-1})$	$1/n_F$	$R^2$	
2107.4	0.28	0.9049	
Sips isotherm			
$K_S$	$q_S (\mu\text{g/g})$	$1/n_S$	$R^2$
0.28	47,475	0.03	0.9877

**Figure 8.**  $\ln k_2$  vs.  $1/T$ .

Based on linear dependence depicted in Figure 8, it was calculated the activation energy value (7.46 kJ/mol), which was below 40 kJ/mol, shows us that the studied adsorption process is a physical one [72].

### 3.2.5. Equilibrium Studies

The adsorption mechanism was established by modelling experimental data with three different isotherms: Langmuir, Freundlich and Sips (obtained data being presented in Figure 9). Isotherms are applied to model obtained experimental data to determine the maximum adsorption capacity of the material. The Freundlich isotherm model assumes that the surface area of the material with adsorbent properties is heterogeneous, so it can be considered that the heat distribution required for the adsorption process on the surface of the adsorbent material is uneven and multilayer adsorption can occur due to unlimited active centres. The Sips isotherm is derived from the Langmuir and Freundlich isotherms. In the case of low adsorbate concentrations, it is reduced to the Freundlich isotherm and, if the adsorbate concentrations are high, it has the characteristics of the Langmuir isotherm. Therefore, this isotherm can be used to calculate the adsorption capacity.

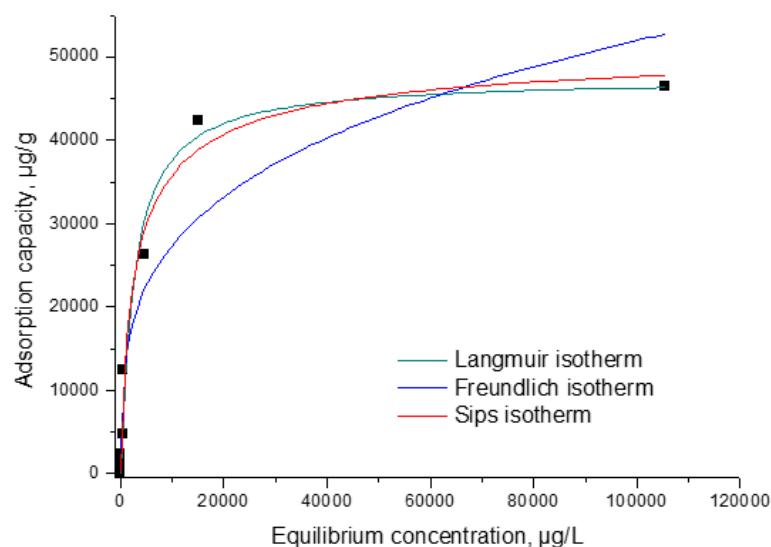


**Figure 9.** Equilibrium studies.

From the data presented in Figure 9 were evaluated the specific parameters associated with each isotherm used for modelling the experimental, parameters depicted in Table 4.

The relationship between the equilibrium concentration ( $C_e$ ) of In (III) and the adsorption capacity demonstrates that as the equilibrium concentration increases, so does the adsorption capacity until equilibrium is reached, establishing the maximum adsorption capacity obtained experimentally,  $q_{e,exp}$  (~46.4 mg In (III)/g). It was found, according to the data in Table 5, that the model that best describes the adsorption process is the Sips one, because the regression coefficient,  $R^2$ , is closest to 1 ( $R^2 = 0.9877$ ), and the theoretical adsorption capacity ~47.5 mg In (III)/g is near the experimental one. Taking in account the data presented in the literature, a comparison of the adsorption capacity obtained for the new prepared material for the recovery of In (III) with adsorption capacity obtained for other materials is presented in Table 5. Based on presented data it was found that the material  $MgFe_2O_4$  present highest adsorption capacity.

**Table 5.** Comparison of adsorption performance with other material for In (III) adsorption.

Materials	$q$ , mg/g	References
Cellulose with iminodiacetic acid	0.172	[70]
CCB	7.89	[14]
Amberlite IRA-400AR	14.93	[73]
Coated solvent impregnated resins	23.8	[74]
Modified solvent impregnated resins	26.25	[10]
Dowex 1	31.00	[73]
Modified solvent impregnated resin (MSIR—impregnation of sec-octylphenoxy acetic acid (CA-12) on styrene–divinylbenzene copolymer support (HZ818) after nitration of the benzene rings)	26.0	[10]
Non-imprinted polymers In(III)-NIP	29.75	[2]
LewatitTP 260	1.437	[7]
Lewatit TP 208	1.488	[7]
Amberlite IRA 743	0.84	[7]
$MgFe_2O_4$	~46.4	This paper

### 3.2.6. Thermodynamic Studies

In order to evaluate the value of Gibbs free energy were performed thermodynamic studies in the temperature range 298–328K, by using the Gibbs–Helmholtz equation. Based on the van't Hoff equation and from the equation of the line obtained from the graphical representation of  $\ln K_d = f(1/T)$ , according to Figure 10, one can calculate the standard variation of the entropy  $\Delta S^\circ$  and the standard variation of the enthalpy  $\Delta H^\circ$ .

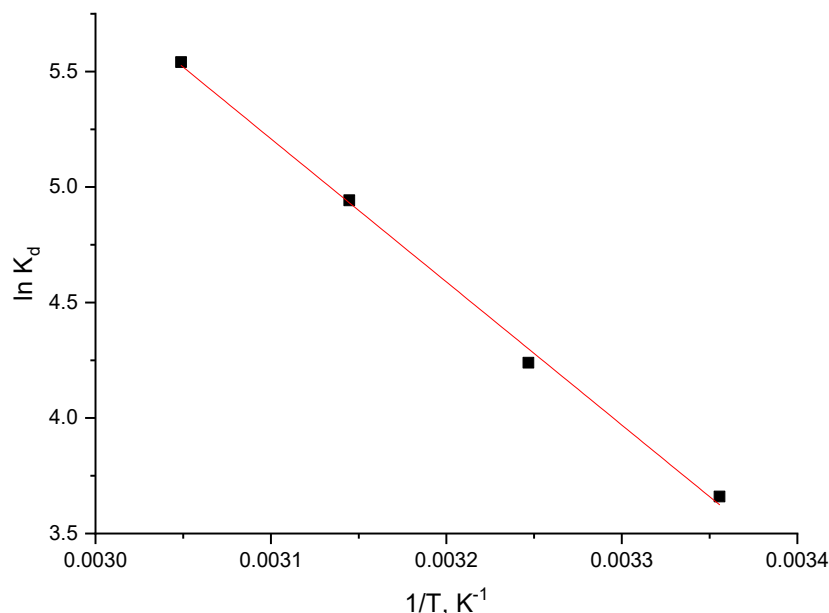


Figure 10. Thermodynamic studies.

Table 6 shows the thermodynamic parameters resulting from the three temperatures.

Table 6. Thermodynamic parameters for adsorption of In (III) onto MgFe<sub>2</sub>O<sub>4</sub>.

$\Delta H^\circ$ (J mol <sup>-1</sup> )	$\Delta S^\circ$ (J mol <sup>-1</sup> K <sup>-1</sup> )	$\Delta G^\circ$ (kJ mol <sup>-1</sup> )				$R^2$
		298 K	308 K	318 K	328 K	
51.52	203.0	−60.44	−62.47	−64.50	−66.53	0.9975

From the resulting data, it is observed that  $\Delta H^\circ$  has a positive value, meaning that the studied adsorption is endothermic. It is also observed that  $\Delta G^\circ$  has negative values, increasing in absolute value with temperature increase, indicating that the adsorption process is spontaneous and influenced by temperature. The value of  $\Delta S^\circ$  is positive which indicates that the adsorption process is favoured, flowing at the interface of the material MgFe<sub>2</sub>O<sub>4</sub>/solution with In (III).

An important aspect is that it is represented by the ability to reuse the new adsorbent material. After indium adsorption, the exhausted material was treated with 15% HCl in order to regenerate it. In this way, spinel type adsorbent material was reused 11 times.

## 4. Conclusions

Obtained experimental data prove that the new prepared adsorbent material (MgFe<sub>2</sub>O<sub>4</sub>) can be used with good results for the recovery by adsorption of indium from aqueous solutions. The MgFe<sub>2</sub>O<sub>4</sub> composite was synthesized by the sol-gel method and further characterized by thermogravimetric analysis, Fourier transform infrared spectroscopy and X-ray analysis. The purpose of these analyses was to highlight the formation by heat treatment of magnesium ferrite, MgFe<sub>2</sub>O<sub>4</sub>, predominantly and as a secondary phase magnetite. Based on experimental data obtained after performing these analyses we can conclude

that the new prepared adsorbent material is preponderantly represented by magnesium ferrite. Further,  $\text{MgFe}_2\text{O}_4$  was used in the adsorption experiment in order to recover In ions from aqueous solutions. As a result of the adsorption experiment, we established the working conditions needed to obtain the best adsorption capacity of the material used for In (III) recovery from aqueous solutions. In this context, optimum conditions are:  $\text{pH} > 2$ , contact time 90 min, temperature 298 K, initial concentration  $200 \text{ mg L}^{-1}$ . By conducting the adsorption process in optimal conditions we obtained a maximum adsorption capacity of 46.4 mg of In (III) per each gram of adsorbent material. The mechanism of the adsorption process has been highlighted by kinetic, thermodynamic and equilibrium studies. Taking into account the obtained experimental data we can conclude that the studied adsorption is homogeneous, spontaneous, endothermic and temperature-dependent. Based on the Weber and Morris model we can conclude that the In (III) ions takes place at the  $\text{MgFe}_2\text{O}_4/\text{In (III)}$  solution–material interface.

**Author Contributions:** Investigation, L.C., M.C., P.I., C.I. and N.S.N.; Methodology, P.N.; Supervision, A.N. and P.N.; Validation, N.D.; Writing—original draft, A.N.; Writing—review & editing, N.D. All authors have read and agreed to the published version of the manuscript.

**Funding:** This work was supported by a grant of the Romanian Ministry of Research, Innovation and Digitalization, project number PFE 26/30.12.2021, PERFORM-CDI@UPT<sup>100</sup>—*The increasing in the performance of the Polytechnic University of Timișoara by strengthening the research, development and technological transfer capacity in the field of “Energy, Environment and Climate Change” at the beginning of the second century of its existence*, within Program 1—Development of the national system of Research and Development, Subprogram 1.2—Institutional Performance—Institutional Development Projects—Excellence Funding Projects in RDI, PNCDI III.

**Institutional Review Board Statement:** Not applicable.

**Conflicts of Interest:** The authors declare no conflict of interest.

## References

1. Adhikari, B.B.; Gurung, M.; Kawakita, H.; Ohto, K. Solid phase extraction, preconcentration and separation of indium with methylene crosslinked calix[4]- and calix[6]arene carboxylic acid resins. *Chem. Eng. Sci.* **2012**, *78*, 144–154. [\[CrossRef\]](#)
2. Li, M.; Feng, C.; Li, M.; Zeng, Q.; Gan, Q. Synthesis and application of a surface-grafted In (III) ion-imprinted polymer for selective separation and pre-concentration of indium (III) ion from aqueous solution. *Hydrometallurgy* **2015**, *154*, 63–71. [\[CrossRef\]](#)
3. Li, G.; Zhang, B.; Ma, Z.; Wang, Z. Facile synthesis of hydroxyl- and amine-riched porous polymer for indium recovery in water. *Microporous Mesoporous Mater.* **2021**, *323*, 111162. [\[CrossRef\]](#)
4. Duan, H.; Wang, J.; Liu, L.; Huang, Q.; Li, J. Rethinking China’s strategic mineral policy on indium: Implication for the flat screens and photovoltaic industries. *Prog. Photovolt. Res. Appl.* **2016**, *24*, 83–93. [\[CrossRef\]](#)
5. Díez, E.; Gómez, J.M.; Rodríguez, A.; Bernabé, I.; Sáez, P.; Galán, J. A new mesoporous activated carbon as potential adsorbent for effective indium removal from aqueous solutions. *Microporous Mesoporous Mater.* **2020**, *295*, 109984. [\[CrossRef\]](#)
6. Zimmermann, Y.-S.; Niewersch, C.; Lenz, M.; Kül, Z.Z.; Corvini, P.F.-X.; Schäffer, A.; Wintgens, T. Recycling of Indium From CIGS Photovoltaic Cells: Potential of Combining Acid-Resistant Nanofiltration with Liquid–Liquid Extraction. *Environ. Sci. Technol.* **2014**, *48*, 13412–13418. [\[CrossRef\]](#)
7. Assefi, M.; Maroufi, S.; Nekouei, R.K.; Sahajwalla, V. Selective recovery of indium from scrap LCD panels using macroporous resins. *J. Clean. Prod.* **2018**, *180*, 814–822. [\[CrossRef\]](#)
8. Alfantazi, A.; Moskalyk, R. Processing of indium: A review. *Miner. Eng.* **2003**, *16*, 687–694. [\[CrossRef\]](#)
9. Lee, S.-K.; Lee, U.-H. Adsorption and desorption property of iminodiacetate resin (Lewatit®TP207) for indium recovery. *J. Ind. Eng. Chem.* **2016**, *40*, 23–25. [\[CrossRef\]](#)
10. Li, H.; Liu, J.; Gao, X.; Liu, C.; Guo, L.; Zhang, S.; Liu, X.; Liu, C. Adsorption behavior of indium(III) on modified solvent impregnated resins (MSIRs) containing sec-octylphenoxy acetic acid. *Hydrometallurgy* **2012**, *121–124*, 60–67. [\[CrossRef\]](#)
11. Li, J.; Gao, S.; Duan, H.; Liu, L. Recovery of valuable materials from waste liquid crystal display panel. *Waste Manag.* **2009**, *29*, 2033–2039. [\[CrossRef\]](#)
12. Rocchetti, L.; Amato, A.; Fonti, V.; Ubaldini, S.; de Michelis, I.; Kopacek, B.; Vegliò, F.; Beolchini, F. Cross-current leaching of indium from end-of-life LCD panels. *Waste Manag.* **2015**, *42*, 180–187. [\[CrossRef\]](#) [\[PubMed\]](#)
13. Bakry, A.M.; Alamier, W.M.; Salama, R.S.; El-Shall, M.S.; Awad, F.S. Remediation of water containing phosphate using ceria nanoparticles decorated partially reduced graphene oxide (CeO<sub>2</sub>-PRGO) composite. *Surfaces Interfaces* **2022**, *31*, 102006. [\[CrossRef\]](#)
14. Calagui, M.J.C.; Senoro, D.B.; Kan, C.-C.; Salvacion, J.W.; Futralan, C.M.; Wan, M.-W. Adsorption of indium(III) ions from aqueous solution using chitosan-coated bentonite beads. *J. Hazard. Mater.* **2014**, *277*, 120–126. [\[CrossRef\]](#) [\[PubMed\]](#)

15. Limin, Y.; Wenquan, J.; Zhongzhen, F. Purification of indium electrolyte by coprecipitation. *Mater. Rev.* **2011**, *25*, 72–74.
16. Swain, B.; Mishra, C.; Hong, H.S.; Cho, S.-S.; Lee, S.K. Commercial process for the recovery of metals from ITO etching industry wastewater by liquid–liquid extraction: Simulation, analysis of mechanism, and mathematical model to predict optimum operational conditions. *Green Chem.* **2015**, *17*, 3979–3991. [[CrossRef](#)]
17. Gupta, B.; Mudhar, N.; Singh, I. Separations and recovery of indium and gallium using bis(2,4,4-trimethylpentyl)phosphinic acid (Cyanex 272). *Sep. Purif. Technol.* **2007**, *57*, 294–303. [[CrossRef](#)]
18. Lee, M.; Ahn, J.; Lee, E. Solvent extraction separation of indium and gallium from sulphate solutions using D2EHPA. *Hydrometallurgy* **2002**, *63*, 269–276. [[CrossRef](#)]
19. Trochimczuk, A.W.; Czerwińska, S. In(III) and Ga(III) sorption by polymeric resins with substituted phenylphosphinic acid ligands. *React. Funct. Polym.* **2005**, *63*, 215–220. [[CrossRef](#)]
20. Zhang, X.; Yin, G.; Hu, Z. Extraction and separation of gallium, indium and thallium with several carboxylic acids from chloride media. *Talanta* **2003**, *59*, 905–912. [[CrossRef](#)]
21. Yang, J.; Retegan, T.; Ekberg, C. Indium recovery from discarded LCD panel glass by solvent extraction. *Hydrometallurgy* **2013**, *137*, 68–77. [[CrossRef](#)]
22. Wu, M.; Sun, D.D.; Tay, J.H. Effect of operating variables on rejection of indium using nanofiltration membranes. *J. Membr. Sci.* **2004**, *240*, 105–111. [[CrossRef](#)]
23. He, Y.; Ma, E.; Xu, Z. Recycling indium from waste liquid crystal display panel by vacuum carbon-reduction. *J. Hazard. Mater.* **2014**, *268*, 185–190. [[CrossRef](#)] [[PubMed](#)]
24. Medvecký, L.; Briančin, J. Possibilities of simultaneous determination of indium and gallium in binary InGa alloys by anodic stripping voltammetry in acetate buffer. *Chem. Pap.* **2004**, *58*, 93–100.
25. Ferreira, E.D.M.M.; Morelli, T.; Moreira, I.M.N.S.; De Carvalho, M.S. Studies on indium sorption from iodide medium by polyurethane foam. *J. Braz. Chem. Soc.* **2004**, *15*, 563–569. [[CrossRef](#)]
26. Liu, J.S.; He, Z.G.; Cai, J.; Cai, C.G.; Zhou, B.X.; Cai, W.M. Separation of indium (III), gallium (III), and zinc (II) with Levextrel resin containing di(2-ethylhexyl) phosphoric acid (CL-P204): Part I. Selection of separation conditions. *Rare Met.* **2003**, *22*, 235–240.
27. Liu, J.; Chen, H.; Chen, X.; Guo, Z.; Hu, Y.; Liu, C.; Sun, Y. Extraction and separation of In(III), Ga(III) and Zn(II) from sulfate solution using extraction resin. *Hydrometallurgy* **2006**, *82*, 137–143. [[CrossRef](#)]
28. Yuan, Y.; Liu, J.; Zhou, B.; Yao, S.; Li, H.; Xu, W. Synthesis of coated solvent impregnated resin for the adsorption of indium (III). *Hydrometallurgy* **2010**, *101*, 148–155. [[CrossRef](#)]
29. Song, Q.; Liu, Y.; Zhang, L.; Xu, Z. Facile indium recovery from waste liquid crystal displays: Chloride-facilitated indium electroreduction and stepwise Cu/MoO<sub>2</sub> and indium electrodeposition. *J. Hazard. Mater.* **2021**, *415*, 125599. [[CrossRef](#)]
30. Armstrong, R.D.; Todd, M.; Atkinson, J.W.; Scott, K. Selective electrodeposition of metals from simulated waste solutions. *J. Appl. Electrochem.* **1996**, *26*, 379–384. [[CrossRef](#)]
31. Ibrahim, A.A.; Salama, R.S.; El-Hakam, S.A.; Khder, A.S.; Ahmed, A.I. Synthesis of 12-tungstophosphoric acid supported on Zr/MCM-41 composite with excellent heterogeneous catalyst and promising adsorbent of methylene blue. *Colloids Surfaces A Physicochem. Eng. Asp.* **2021**, *631*, 127753. [[CrossRef](#)]
32. Salama, R.S.; El-Sayed, E.-S.M.; El-Bahy, S.M.; Awad, F.S. Silver nanoparticles supported on UiO-66 (Zr): As an efficient and recyclable heterogeneous catalyst and efficient adsorbent for removal of Indigo Carmine. *Colloids Surfaces A Physicochem. Eng. Asp.* **2021**, *626*, 127089. [[CrossRef](#)]
33. Atkins, P.; de Paula, J. *Atkins' Physical Chemistry*; Oxford University Press: Oxford, UK, 2005; p. 1008.
34. de Freitas, F.; Battistola, L.D.; de Andrade, R.L.T. Adsorption of Cu<sup>2+</sup> and Pb<sup>2+</sup> ions by *Pontederia rotundifolia* (L.f.) (Pontederiaceae) and *Salvinia biloba* Raddi (Salviniaceae) Biomass. *Water Air Soil Pollut.* **2018**, *229*, 349. [[CrossRef](#)]
35. Freundlich, H.M.F. Over the adsorption in solution. *J. Phys. Chem.* **1906**, *57*, 385–470.
36. Tuzen, M.; Soylak, M. Chromium speciation in environmental samples by solid phase extraction on Chromosorb 108. *J. Hazard. Mater.* **2006**, *129*, 266–273. [[CrossRef](#)]
37. Fortes, M.; Martins, A.; Benedetto, J. Indium adsorption onto ion exchange polymeric resins. *Miner. Eng.* **2003**, *16*, 659–663. [[CrossRef](#)]
38. Tokuyama, H.; Iwama, T. Solid-phase extraction of indium(III) ions onto thermosensitive poly(N-isopropylacrylamide). *Sep. Purif. Technol.* **2009**, *68*, 417–421. [[CrossRef](#)]
39. Wang, S.; Sun, H.; Ang, H.M.; Tade, M.O. Adsorptive remediation of environmental pollutants using novel graphene-based nanomaterials. *Chem. Eng. J.* **2013**, *226*, 336–347. [[CrossRef](#)]
40. Tuzen, M.; Soylak, M. A solid phase extraction procedure for Indium prior to its graphite furnace atomic absorption spectrometric determination. *J. Hazard. Mater.* **2006**, *129*, 179–185. [[CrossRef](#)]
41. Hoogerstraete, T.V.; Onghena, B.; Binnemans, K. Homogeneous Liquid–Liquid Extraction of Metal Ions with a Functionalized Ionic Liquid. *J. Phys. Chem. Lett.* **2013**, *4*, 1659–1663. [[CrossRef](#)]
42. Liu, H.-M.; Wu, C.-C.; Lin, Y.-H.; Chiang, C.-K. Recovery of indium from etching wastewater using supercritical carbon dioxide extraction. *J. Hazard. Mater.* **2009**, *172*, 744–748. [[CrossRef](#)] [[PubMed](#)]
43. Bossche, A.V.D.; Vereycken, W.; Hoogerstraete, T.V.; Dehaen, W.; Binnemans, K. Recovery of Gallium, Indium, and Arsenic from Semiconductors Using Tribromide Ionic Liquids. *ACS Sustain. Chem. Eng.* **2019**, *7*, 14451–14459. [[CrossRef](#)]

44. Ozkantar, N.; Yilmaz, E.; Soylak, M.; Tuzen, M. Solid-phase extraction of iridium from soil and water samples by using activated carbon cloth prior to its spectrophotometric determination. *Environ. Monit. Assess.* **2015**, *187*, 501. [[CrossRef](#)]
45. Memon, F.N.; Ayyilidiz, H.F.; Kara, H.; Memon, S.; Kenar, A.; Leghari, M.K.; Topkafa, M.; Sherazi, S.T.H.; Memon, N.A.; Durmaz, F.; et al. Application of central composite design for the optimization of on-line solid phase extraction of  $\text{Cu}^{2+}$  by calix[4]arene bonded silica resin. *Chemom. Intell. Lab. Syst.* **2015**, *146*, 158–168. [[CrossRef](#)]
46. Alguacil, F.; Lopez, F.; Rodriguez, O.; Martinez-Ramirez, S.; Garcia-Diaz, I. Sorption of indium (III) onto carbon nanotubes. *Ecotoxicol. Environ. Saf.* **2016**, *130*, 81–86. [[CrossRef](#)] [[PubMed](#)]
47. Naaz, F.; Dubey, H.K.; Kumari, C.; Lahiri, P. Structural and magnetic properties of  $\text{MgFe}_2\text{O}_4$  nanopowder synthesized via co-precipitation route. *SN Appl. Sci.* **2020**, *2*, 808. [[CrossRef](#)]
48. Bloesser, A.; Kurz, H.; Timm, J.; Wittkamp, F.; Simon, C.; Hayama, S.; Weber, B.; Apfel, U.-P.; Marschall, R. Tailoring the Size, Inversion Parameter, and Absorption of Phase-Pure Magnetic  $\text{MgFe}_2\text{O}_4$  Nanoparticles for Photocatalytic Degradations. *ACS Appl. Nano Mater.* **2020**, *3*, 11587–11599. [[CrossRef](#)]
49. Hammache, Z.; Soukeur, A.; Omeiri, S.; Bellal, B.; Trari, M. Physical and photo-electrochemical properties of  $\text{MgFe}_2\text{O}_4$  prepared by sol gel route: Application to the photodegradation of methylene blue. *J. Mater. Sci. Mater. Electron.* **2019**, *30*, 5375–5382. [[CrossRef](#)]
50. Becker, A.; Kirchberg, K.; Marschall, R. Magnesium Ferrite ( $\text{MgFe}_2\text{O}_4$ ) Nanoparticles for Photocatalytic Antibiotics Degradation. *Z. Für Phys. Chem.* **2020**, *234*, 645–654. [[CrossRef](#)]
51. Sun, J.R.; Wang, Z.G.; Wang, Y.Y.; Wei, K.F.; Li, F.S. Structure and Magnetic Properties of  $\text{MgFe}_2\text{O}_4$  Nanoparticles Prepared by the Low-Temperature Solid-State Reaction Method. *Mater. Sci. Forum* **2011**, *686*, 316–318. [[CrossRef](#)]
52. Reddy, S.; Swamy, B.E.K.; Chandra, U.; Mahathesha, K.R.; Sathisha, T.V.; Jayadevappa, H. Synthesis of  $\text{MgFe}_2\text{O}_4$  nanoparticles and  $\text{MgFe}_2\text{O}_4$  nanoparticles/CPE for electrochemical investigation of dopamine. *Anal. Methods* **2011**, *3*, 2792–2796. [[CrossRef](#)]
53. Lagergren, S. About the theory of so-called adsorption of soluble substances. *Kungl. Sven. Vetensk. Handl.* **1898**, *24*, 1–39.
54. Ho, Y.-S. Review of second-order models for adsorption systems. *J. Hazard. Mater.* **2006**, *136*, 681–689. [[CrossRef](#)]
55. Ho, Y.S.; McKay, G. A Comparison of Chemisorption Kinetic Models Applied to Pollutant Removal on Various Sorbents. *Process Saf. Environ. Prot.* **1998**, *76*, 332–340. [[CrossRef](#)]
56. Weber, W.J.; Morris, J.C. Kinetics of Adsorption on Carbon from Solution. *J. Sanit. Eng. Div.* **1963**, *89*, 31–59. [[CrossRef](#)]
57. Weber, W.J.; Morris, J.C. Equilibria and Capacities for Adsorption on Carbon. *J. Sanit. Eng. Div.* **1964**, *90*, 79–108. [[CrossRef](#)]
58. Langmuir, I. The adsorption of gases on plane surfaces of glass, mica and platinum. *J. Am. Chem. Soc.* **1918**, *40*, 1361–1403. [[CrossRef](#)]
59. Sips, R. On the Structure of a Catalyst Surface. *J. Chem. Phys.* **1948**, *16*, 490–495. [[CrossRef](#)]
60. Maensiri, S.; Sangmanee, M.; Wiengmoon, A. Magnesium Ferrite ( $\text{MgFe}_2\text{O}_4$ ) Nanostructures Fabricated by Electrospinning. *Nanoscale Res. Lett.* **2008**, *4*, 221–228. [[CrossRef](#)]
61. Upadhyay, S.; Sreenivas, K. Comparative Studies of  $\text{MgFe}_2\text{O}_4$  Nanoparticles Synthesized using Different Precursors by Sol Gel Auto Combustion Method. *J. At. Mol. Condens. Nano Phys.* **2015**, *2*, 101–108. [[CrossRef](#)]
62. Ilhan, S.; Izotova, S.G.; Komlev, A.A. Synthesis and characterization of  $\text{MgFe}_2\text{O}_4$  nanoparticles prepared by hydrothermal decomposition of co-precipitated magnesium and iron hydroxides. *Ceram. Int.* **2015**, *41*, 577–585. [[CrossRef](#)]
63. Nicola, R.; Costişor, O.; Ciopec, M.; Negrea, A.; Lazău, R.; Ianăşi, C.; Picioruş, E.-M.; Len, A.; Almásy, L.; Szerb, E.I.; et al. Silica-Coated Magnetic Nanocomposites for  $\text{Pb}^{2+}$  Removal from Aqueous Solution. *Appl. Sci.* **2020**, *10*, 2726. [[CrossRef](#)]
64. Sepahvand, R. Synthesis and Characterization of Carbon Nanotubes Decorated with Magnesium Ferrite ( $\text{MgFe}_2\text{O}_4$ ) Nanoparticles by Citrate-Gel Method. *J. Sci. Islam. Repub. Iran* **2011**, *22*, 177–182. [[CrossRef](#)]
65. Pradeep, A.; Priyadharsini, P.; Chandrasekaran, G. Sol-gel route of synthesis of nanoparticles of  $\text{MgFe}_2\text{O}_4$  and XRD, FTIR and VSM study. *J. Magn. Magn. Mater.* **2008**, *320*, 2774–2779. [[CrossRef](#)]
66. Robles, J. *The Engineering of Pt/Carbon Catalyst Preparation-For Application on Proton Exchange Fuel Cell Membrane*; University of Illinois at Chicago: Chicago, IL, USA, 2004.
67. Vidal, C.; do Nascimento, R.; Raulino, G.; Clecius, A.; Melo, D. *Adsorção: Aspectos Teóricos e Aplicações Ambientais*; Imprensa Universitária: Fortaleza, Brazil, 2014.
68. Werner, A.; Rieger, A.; Mosch, M.; Haseneder, R.; Repke, J.-U. Nanofiltration of indium and germanium ions in aqueous solutions: Influence of pH and charge on retention and membrane flux. *Sep. Purif. Technol.* **2017**, *194*, 319–328. [[CrossRef](#)]
69. Baes, C.F.; Mesmer, R.S. The Hydrolysis of Cations. *Ber. Der Bunsenges. Für Phys. Chem.* **1977**, *81*, 245–246.
70. Akama, Y.; Suzuki, S.; Monobe, Y. Study on the adsorption and selective separation of indium from zinc with chelating cellulose. *Cellul. Chem. Technol.* **2016**, *50*, 147–152.
71. Zhang, S.; Ning, S.; Liu, H.; Zhou, J.; Wang, S.; Zhang, W.; Wang, X.; Wei, Y. Highly-efficient separation and recovery of ruthenium from electroplating wastewater by a mesoporous silica-polymer based adsorbent. *Microporous Mesoporous Mater.* **2020**, *303*, 110293. [[CrossRef](#)]
72. Zhang, Y.; Yu, F.; Cheng, W.; Wang, J.; Ma, J. Adsorption Equilibrium and Kinetics of the Removal of Ammoniacal Nitrogen by Zeolite X/Activated Carbon Composite Synthesized from Elutrilithe. *J. Chem.* **2017**, *2017*, 1–9. [[CrossRef](#)]

73. Marinho, R.S.; da Silva, C.N.; Afonso, J.C.; da Cunha, J.W.S.D. Recovery of platinum, tin and indium from spent catalysts in chloride medium using strong basic anion exchange resins. *J. Hazard. Mater.* **2011**, *192*, 1155–1160. [[CrossRef](#)]
74. Kwak, N.-S.; Baek, Y.; Hwang, T.S. The synthesis of poly(vinylphosphonic acid-co-methacrylic acid) microbeads by suspension polymerization and the characterization of their indium adsorption properties. *J. Hazard. Mater.* **2012**, *203–204*, 213–220. [[CrossRef](#)] [[PubMed](#)]